Vol 15 No 6, June 2006
1009-1963/2006/15(06)/1315-05

Chinese Physics

© 2006 Chin. Phys. Soc.
and IOP Publishing Ltd

# Finite element analysis of stress and strain distributions in InAs/GaAs quantum dots*

Zhou Wang-Min(周旺民)[a)b)], Wang Chong-Yu(王崇愚)[b)c)],
Chen Yong-Hai(陈涌海)[d)], and Wang Zhan-Guo(王占国)[d)]

[a)] *College of Mechanical & Electrical Engineering, Zhejiang University of Technology, Hangzhou* 310032, *China*
[b)] *Institute of Functional Materials, Central Iron & Steel Research Institute, Beijing* 100081, *China*
[c)] *Department of Physics, Tsinghua University, Beijing* 100084, *China*
[d)] *Key Laboratory of Semiconductor Materials Science, Institute of Semiconductors, Chinese Academy of Sciences, Beijing* 100083, *China*

(Received 22 November 2005; revised manuscript received 23 March 2006)

In this paper, we perform systematic calculations of the stress and strain distributions in InAs/GaAs truncated pyramidal quantum dots (QDs) with different wetting layer (WL) thickness, using the finite element method (FEM). The stresses and strains are concentrated at the boundaries of the WL and QDs, are reduced gradually from the boundaries to the interior, and tend to a uniform state for the positions away from the boundaries. The maximal strain energy density occurs at the vicinity of the interface between the WL and the substrate. The stresses, strains and released strain energy are reduced gradually with increasing WL thickness. The above results show that a critical WL thickness may exist, and the stress and strain distributions can make the growth of QDs a growth of strained three-dimensional island when the WL thickness is above the critical value, and FEM can be applied to investigate such nanosystems, QDs, and the relevant results are supported by the experiments.

**Keywords:** quantum dots, strain and stress distribution, strain energy, finite element method
**PACC:** 6855, 8190, 6220, 6220D

## 1. Introduction

The nanoscale semiconductor materials are the foundation of advanced quantum devices, and have shown very important application prospects for nanoelectronics and optoelectronics, because quantum confinement effects become not only important, but also designable to a large degree. The formation of self-assembled quantum dots (QDs) in lattice mismatched systems by the Stranski–Krastanov (S-K) growth mode has attracted much attention since these defect-free QDs are expected to lead to a major development of nanoscale optoelectronic devices in future.[1−5] The stress and strain distribution in a growing sample is one of the main driving forces leading to the formation of nanostructures, and influences the particularities of their growth and mutual arrangement.[6−8] However, in the initial stage of heteroepitaxial growth, QDs nucleation on a substrate is random, whose size, density and position in space are very difficult to control. To fabricate the quantum devices for applications by the S-K growth mode, the strain and stress distributions in and around QDs should be known clearly and theoretically, and can be controlled experimentally; one of the major goals of all these understandings is to have the ability to grow QDs in a controlled fashion.

A variety of methods have been used to study the stress and strain distributions in and around QDs. Grundmann *et al*[9] used continuum elasticity and a finite-difference method. Pryor *et al*[10] performed numerical valence force field (VFF) calculations for yielding the equilibrium atomic positions and compared their results with numerical continuum calculations. Andreev *et al* used the Green's function method to obtain several results for inclusions of various simple specific shapes in the anisotropic elasticity case; but for pyramids, they gave only the Fourier transform of the strain fields.[11] Their work was extended later by Pearson and Faux,[12] who gave analytical expressions for the strain fields by assuming isotropic elastic-

*Project supported by the National Natural Science Foundation of China (Grant No 90101004) and by the National Basic Research Program of China (Grant No G2000067102).

ity. These are apparently the only analytical formulas yet available for the strain fields of a pyramidal inclusion, but they can be applied only in an infinite matrix. In the half-space case, the results available are the numerical finite element calculation of Benabbas *et al* for a specific type of square-based InAs QDs in a GaAs matrix [13] and the work of Jogai, in which coupled QDs were discussed.[14]

The finite element method (FEM) is the most effective method for treating complicated geometries among these methods. In the present paper, we perform some systematic calculations of the stress and strain distributions in InAs/GaAs QDs with their shape and dimension as referred to in the experiments of self-assembled QDs,[15,16] and different wetting layer (WL) thickness, using FEM based on anisotropic theory of elasticity. The relevant results are supported by the experiments.

## 2. Theory of elasticity and finite element method

InAs and GaAs, as the important semiconductor materials, are of zincblende crystal structure, which belongs to the cubic system. The elastic deformation follows the anisotropic theory of elasticity:

Equilibrium equations:

$$\sigma_{ij,j} + F_i = 0; \tag{1}$$

Equations of deformation geometry:

$$\varepsilon_{ij} = (u_{i,j} + u_{j,i})/2; \tag{2}$$

Constitutive equations:

$$\sigma_{xx} = C_{11}\varepsilon_{xx} + C_{12}(\varepsilon_{yy} + \varepsilon_{zz}), \tag{3}$$

$$\sigma_{yy} = C_{11}\varepsilon_{yy} + C_{12}(\varepsilon_{xx} + \varepsilon_{zz}), \tag{4}$$

$$\sigma_{zz} = C_{11}\varepsilon_{zz} + C_{12}(\varepsilon_{yy} + \varepsilon_{xx}), \tag{5}$$

$$\sigma_{ij} = 2C_{44}\varepsilon_{ij}, \quad (i \neq j). \tag{6}$$

Here $\sigma_{ij}$, $\varepsilon_{ij}$ and $u_i$ denote the stress, strain and displacement respectively, and $\sigma_{ij,j}$ $(u_{i,j})$ denotes the derivative of $\sigma_{ij}$ $(u_i)$ with respect to the variable $j$; $F_i$ is the component of body force $(i, j = x, y, z)$ and $C_{ij}$ the elastic constant. The crystal constants and elastic constants of InAs and GaAs are listed in Table 1.

**Table 1.** The crystal constants and elastic constants of InAs and GaAs[9].

| | $a_0$/nm | $C_{11}/10^{10}$Pa | $C_{12}/10^{10}$Pa | $C_{44}/10^{10}$Pa |
|---|---|---|---|---|
| InAs | 0.60584 | 8.3 | 4.5 | 4.0 |
| GaAs | 0.56533 | 12.2 | 5.5 | 6.0 |

The FEM of elasticity theory is based on the minimum potential energy principle:

The actual displacements minimize the total potential energy, which is the sum of potential energies from the deformation and external forces:

$$\prod(u_x, u_y, u_z) = \iiint_V (U - F_i u_i)\,\mathrm{d}V - \iint_{S_\sigma} P_i u_i \mathrm{d}S, \tag{7}$$

among the total admissible displacement functions satisfying the displacement boundary conditions. Here $U = \frac{1}{2}\sigma_{ij}\varepsilon_{ij}$ is the strain energy density, $P_i$ the applied stress on the stress boundary $S_\sigma$.

The FEM calculations provide nodal displacements for calculating strain and stress distributions, which satisfy the following linear algebraic equation:

$$\boldsymbol{K}\boldsymbol{u} = F, \tag{8}$$

where $\boldsymbol{u}$ is the vector of nodal displacements, $\boldsymbol{K}$ the stiffness matrix, $\boldsymbol{F}$ the vector of nodal forces, which permit calculation of the complete strain and stress tensors.

## 3. The stress and strain distributions in and around QDs

Now we consider InAs truncated pyramid QDs on a thin InAs layer (WL) within GaAs (substrate) (Fig.1) according to the experiment observed by molecular-beam epitaxy (MBE) and transmission electron microscopy (TEM).[15,16]

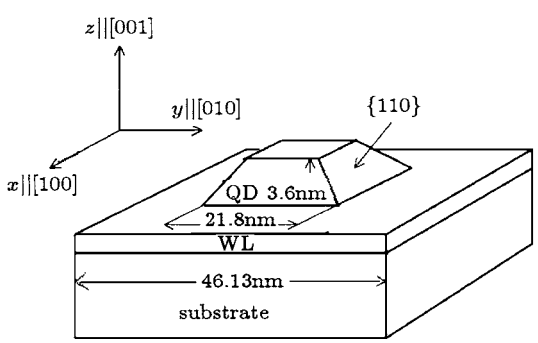



**Fig.1.** Schematic drawing of the dot geometry. The origin of coordinates is at the centre of the upper interface of the WL.

The WL thickness is chosen to take values of 1.6, 1.7, 1.8, 1.9 and 2.0 monolayers (ML); the base length of the QD is 21.8nm, its height is 3.6nm, and the lengths of the substrate and WL are 46.13nm. In order to obtain the three-dimensional stress and strain

distributions in the system, we perform a numerical calculation using FEM, in which the total potential energy of the structures in the elastic continuum theory is minimized by variation with respect to nodal displacements. In FEM calculations, the geometry is meshed with 8-node hexahedron elements, 162208 elements and 188642 nodes are involved, taking into account the crystal structure. The lateral displacement boundary conditions of the QDs and WL are determined in the light of the misfit $\varepsilon \approx 7\%$ between InAs and GaAs, the displacements are zero for positions far away from the substrate, and the top surface of QDs is stress free.

The FEM calculations show:

1) The normal stress $\sigma_{xx}\,(\sigma_{yy})$ in $x$ $(y)$-direction, whose maximum (pressure) is concentrated at the vicinity of the lateral boundaries of the WL and QDs, which is reduced gradually from the boundaries to the interior, and tends to a uniform state for the places away from the lateral boundaries of the QDs about $2.5a_0$. Figure 2 shows the distribution of stress $\sigma_{xx}$ on the upper surface of the WL along a [100] line passing through the origin of the coordinates.

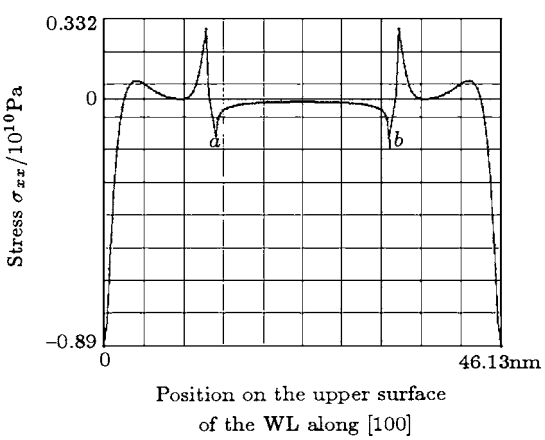



**Fig.2.** Distribution of stress $\sigma_{xx}$ on the upper surface of WL along a [100] line passing through the origin. The curve ab shows the stress distribution of the QDs base along the line [100].

The normal stress $\sigma_{zz}$ in the $z$-direction, whose maximum (tension) occurs at the vicinity of the boundary of the substrate near the WL, and extends to about $0.6a_0$; the maximal pressure occurs at the lower part of the substrate, and decreases gradually along the growth direction of the QDs. Figure 3 gives the stress distribution for a line scanning in the direction [001] passing through the centre of the QD top surface.

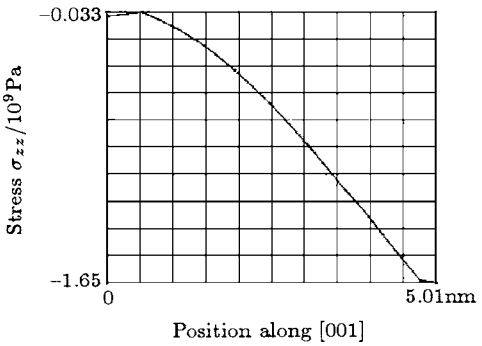



**Fig.3.** Distribution of stress $\sigma_{zz}$ for a line scanning in the direction [001] passing through the centre of the QD top surface.

The shear stress $\sigma_{xy}$ is uniform on the whole. The maximal shear stress $\sigma_{zx}\,(\sigma_{yz})$ occurs at the vicinity of the interface between the WL and substrate; the stress is weakened gradually from the interface to the interior and approaches a uniform state at the positions away from the boundary about $3.5a_0$–$4.0a_0$.

2) The strain $\varepsilon_{xx}\,(\varepsilon_{yy})$ in the $x$ $(y)$-direction, whose maximum (contraction) occurs at the vicinity of the lateral boundaries of the WL and QDs, which is weakened gradually from the boundaries to the interior, and approaches a uniform state for the positions away from the boundary about $3.0a_0$. Figure 4 shows the strain distribution on the upper surface of the WL along a [100] line passing through the origin of the coordinates.

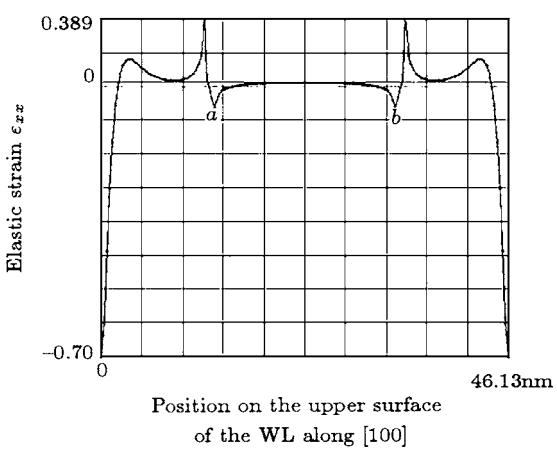



**Fig.4.** Distribution of strain $\varepsilon_{xx}$ on the upper surface of WL along a [100] line passing through the origin. The curve ab is the strain distribution on the QD's base along the line [100].

The maximal elongation of the$\varepsilon_{zz}$ in the $z$-direction appears at the vicinity of the boundaries of the substrate near the WL, and extends to about $1.0a_0$; and the maximal contraction is at the lower part of the substrate. Figure 5 shows the strain distribution for a line scanning in the direction [001] passing through the centre of the QD top surface.

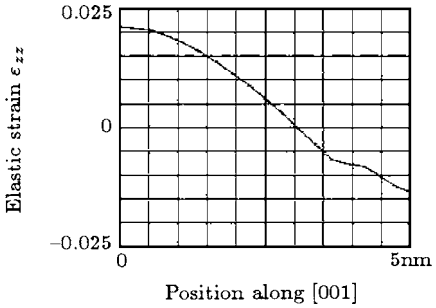



**Fig.5.** Distribution of strain $\varepsilon_{zz}$ for a line scanning in the direction [001] passing through the centre of the QD top surface.

The characteristics of shear strain distributions are the same as those of the shear stresses. The stresses and strains are weakened slightly with increasing WL thickness.

3) The elastic strain energy is mainly concentrated at the vicinity of the interface between the WL and substrate, and the energy density tends to be uniform in other regions.

The intrinsic strains induced by lattice misfit are

$$\varepsilon_{ij}^0 = -\chi\delta_{ij}\varepsilon, \tag{9}$$

where $i, j = x, y$; $\chi = 1$ in the epitaxial material and $\chi = 0$ in the substrate.

The total strain energy in the coherent equilibrium state after elasticity relaxation is[17]

$$\begin{aligned} E_{\text{equi}} &= \frac{1}{2}\int_V \sigma_{ij}(\varepsilon_{ij} - \varepsilon_{ij}^0)\mathrm{d}V \\ &= -\frac{1}{2}\int_V \sigma_{ij}\varepsilon_{ij}^0\mathrm{d}V - \left(-\frac{1}{2}\int_V \sigma_{ij}\varepsilon_{ij}\mathrm{d}V\right). \end{aligned} \tag{10}$$

We define the misfit strain energy induced by the intrinsic strains as

$$E_{\text{misfit}} = -\frac{1}{2}\int_V \sigma_{ij}\varepsilon_{ij}^0\mathrm{d}V, \tag{11}$$

and the released strain energy

$$E_{\text{release}} = -\frac{1}{2}\int_V \sigma_{ij}\varepsilon_{ij}\mathrm{d}V, \tag{12}$$

The calculations show that the released elastic strain energy

$$E_{\text{release}} = E_{\text{misfit}} - E_{\text{equi}}, \tag{13}$$

due to the coherent elasticity relaxation, is reduced gradually with increasing WL thickness in the systems. The approximate values of the released strain energy in the systems with different WL thickness are given in Table 2.

**Table 2.** The released strain energy values of the systems with different WL thickness.

| WL thickness/ML | 1.6 | 1.7 | 1.8 | 1.9 | 2.0 |
|---|---|---|---|---|---|
| Strain energy/eV | 63635.00 | 58652.63 | 54908.94 | 52019.31 | 49792.19 |

Note that Figs.2–5 are the plots of the stress and strain distributions in the system with the WL thickness being 1.6ML. The variations of different WL thickness have little effect on the strain and stress fields in the QDs. From Figs.2 and 4, the stress $\sigma_{xx}$ and strain $\varepsilon_{xx}$ approach zero in the central zone, indicating that the QD is almost relaxed in the zone.

# 4. Conclusion and discussion

The growth models of the QDs we choose are based on the experiments. The results show that the stress and strain distributions (the stress and strain concentration at the boundaries) can lead the growth of QDs to a growth of strained three-dimensional islands when the deposited layer thickness is above a critical thickness. The fact that the thinner the WL, the larger the released strain energy, or the lower the total strain energy stored in the systems, implies that there may be a critical WL thickness for the growth of the defect-free and island-shaped QDs. In addition, we have performed FEM calculations of the model with the WL thickness being 1.5 ML, and found that the deformation induced by lattice-misfit of the system is no longer the coherent elastic strain, but an elasto-plastic mechanical strain, e.g., the elastic energy is partly reduced by misfit dislocations formed at the substrate/layer interface (the quantitative result is not presented here, because, to the best of our knowledge, there have not been experimental yield stress values of the semiconductor materials, such as InAs and GaAs, for calculating the plastic strain): namely, this defect-free QDs does not exist. The critical thickness of dislocation-free InAs film on GaAs is about 2 ML according to Ref.[18]. In other words, the growth

of defect-free QDs must be the plane growth when the epilayer thickness is less than the critical thickness; and it must be the island-shaped growth because the atoms move by diffusion, in which the strain energy stored in the system is reduced, when the film thickness is larger than the thickness. From the above discussion, we can deduce that the critical WL thickness is about 1.6 ML from the energetic and logic reasoning, this is in good agreement with the atomic force microscopy (AFM) and reflection high-energy electron diffraction (RHEED) measurements.[19−21] This explains the growth process and mechanism of the defect-free QDs in terms of strain. Meanwhile, the results also show that FEM can be extended to the investigation of nanosystems, QDs, and the relevant results are supported by experiments. The QDs with more complicated geometry, such as bounded by at least ten facets, four of which determine the shape and are in {137} orientation,[22] also can be explored by the method.

## References


[1] Guha S, Madhukbr A and Rajkumar K C 1990 *Appl. Phys. Lett.* **57** 2110

[2] Leonard D, Krishnamurthy M, Reaves C M, Denbaars S P and Petroff P M 1993 *Appl. Phys. Lett.* **63** 3203

[3] Moison J M, Houzay F, Barthe F, Leprince L, Andre E and Vatel O 1994 *Appl. Phys. Lett.* **64** 196

[4] Brus L 1993 *IEEE J. Quantum Electron.* **22** 1909

[5] Asada M, MiyAmoto Y and Suematsu Y 1986 *IEEE J. Quantum Electron.* **22** 1915

[6] Stangl J, Holy V and Bauer G. 2004 *Rev. Mod. Phys.* **76** 725

[7] Wang X P, Xie F, Shi Q W and Zhao T X 2004 *Acta Phys. Sin.* **53** 2699 (in Chinese)

[8] Meng Y and Zhang Q Y 2005 *Acta Phys. Sin.* **54** 5804 (in Chinese)

[9] Grundmann M, Stier O and Bimberg D 1995 *Phys. Rev.* B **52** 11969

[10] Pryor C, Kim J, Wang L W, Williamson A J and Zunger A 1998 *J. Appl. Phys.* **83** 2548

[11] Andreev A D, Downes J R, Faux D A and O'Reilly E P 1999 *J. Appl. Phys.* **86** 297

[12] Pearson G S and Faux D A 2000 *J. Appl. Phys.* **88** 730

[13] Benabbas T, Androussi Y and Lefebvre A 1999 *J. Appl. Phys.* **86** 1945

[14] Jogai B 2000 *J. Appl. Phys.* **88** 5050

[15] Grundmann M, Christen J, Ledentsov N N, Böhrer J, Bimberg D, Ruvimov S S, Werner P, Richter U, Gösele U, Heydenreich J, Ustinov V M, Yu A Egorov, Zhukov A E, Kop'ev P S and Alferov Zh I 1995 *Phys. Rev. Lett.* **74** 4043

[16] Liu H.Y, Xu B, Chen Y H and Wang Z G *2000 J. Appl. Phys.* **88** 5433

[17] Ipatova I P, Malyshkin V G. and Shchukin V A 1993 *J. Appl. Phys.* **74** 7198

[18] Jesser W A and Kuhlmann-Wilsdorf D 1967 *Phys. Stat. Sol.* **19** 95

[19] Kobayashi N P, Ramachandran T R, Chen P and Madhukar A 1996 *Appl. Phys. Lett.* **68** 3299

[20] Heyn Ch 2001 *Phys. Rev.* B **64** 165306

[21] Garcia J M, Silveira J P and Briones F 2000 *Appl. Phys. Lett.* **77** 409

[22] Marquez J, Geelhaar L and Jacobi K 2000 *Appl. Phys. Lett.* **78** 409